

1
2 Microporous and Mesoporous Materials (2019) accepted

3

4 **External surface phenomena in dealumination and desilication of large**
5 **single crystals of ZSM-5 zeolite synthesized from a sustainable source**

6 Deizi V. Peron^{a,b}, Vladimir L. Zholobenko^c, James H. S. de Melo^b, Mickael Capron^a,
7 Nicolas Nuns^a, Michèle Oberson de Souza^b, Liliana A. Feris^b, Nilson R. Marcilio^b, Vitaly
8 V. Ordonsky^a and Andrei Y. Khodakov^{a*}

9

10 ^a*Univ. Lille, CNRS, Centrale Lille, ENSCL, Univ. Artois, UMR 8181 – UCCS – Unité*
11 *de Catalyse et Chimie du Solide, F-59000 Lille, France*

12 ^b*Universidade Federal do Rio Grande do Sul - UFRGS, Porto Alegre, RS 90040-040,*
13 *Brazil*

14 ^c*School of Physical and Chemical Sciences, Keele University, Staffordshire, ST5*
15 *5BG, United Kingdom*

16

17 ^{*}*andrei.khodakov@univ-lille.fr (Corresponding author)*

18

19 **Abstract**

20 Zeolite dealumination and desilication are common methods, which improve
21 accessibility of the active sites located inside the zeolite crystallites and tune the
22 zeolite acidity. The exact mechanism of these post-synthesis zeolite treatments
23 remains under discussion. In this paper, a series of dealuminated and desilicated
24 ZSM-5 zeolites are prepared using single or combined post-synthesis dealumination
25 and desilication of large zeolite single crystals with oxalic acid and sodium
26 hydroxide. The ZSM-5 zeolite has been synthesized using silica extracted from fly
27 ash. Zeolite desilication results in the potholes, leaf-type structures and other clearly
28 visible defects on the surface of zeolite crystallites, while the effect of dealumination
29 is less pronounced. The low temperature nitrogen adsorption suggests the formation
30 of mesopores in the zeolites formed by the voids between and in the irregular zeolite
31 crystallites produced during post-synthesis treatments. ^{27}Al and ^{29}Si MAS NMR in
32 combination with XRD data are indicative of only minor modifications of the bulk
33 zeolite structure during dealumination and desilication. The total Brønsted acidity
34 only slightly decreases and is not affected by the type of zeolite post-synthesis
35 treatment. After desilication of large single crystals of ZSM-5, noticeable
36 enhancement of the Brønsted acidity on the zeolite external surface has been detected
37 by FTIR of absorbed collidine. The zeolites with higher acidity on the external
38 surface have shown higher activity in the anisole acylation with hexanoic acid. A
39 combination of characterization techniques suggests that the dealumination and
40 desilication of the large crystals of ZSM-5 zeolite using post-synthesis treatments
41 respectively with acid and alkali selectively starts at the zeolite external surface.

42

43 **Keywords:** mesoporous zeolite; ZSM-5; post-synthesis; external surface; acidity

44

45 **1. Introduction**

46

47 Zeolites are crystalline microporous aluminosilicates, which are widely used in
48 adsorption, separation and catalysis. Zeolites are synthesized from silica and alumina
49 sources usually in the presence of structure-directing agents, which are also called
50 templates, under hydrothermal conditions. Synthesis of zeolites from fly ash has become
51 increasingly attractive [1,2] in many countries, because of the challenges associated with
52 coal production and fly ash disposal. In Brazil, ~4 million tons of coal ash are produced
53 annually in the thermoelectric and industrial sectors [365]. The often irregular and
54 uncontrolled deposition of this waste causes environmental problems, such as
55 contamination of groundwater, soil and imbalance of ecological systems. Therefore,
56 sustainable applications of fly ash are desirable to mitigate environmental pollution and
57 health hazard. High silica content makes fly ash a suitable feedstock for the production
58 of zeolite materials. The first step in fly ash utilization involves dissolution of the
59 crystalline and amorphous phases of the ash in alkaline medium (NaOH or KOH) in order
60 to make the Si and Al available for the formation of the zeolite framework during
61 crystallization.

62 The benefits of zeolites for many industrial applications arise from their regular
63 crystalline structure, high surface area, developed porosity, high stability, intrinsic acidity
64 and an opportunity to introduce functionalities such as metal cations, metal clusters,
65 organic complexes or enzymes. The acidity type, acid site amount, strength, and possible
66 synergies with other zeolite active sites are extremely important for catalytic applications
67 of zeolite-based materials. The small size of zeolite micropores can result in shape

selectivity effects [6] in catalytic reactions, when the size of the reaction products, intermediates or reagents can be limited by the size of zeolite micropores.

The small pore size of zeolites can also be a drawback, which may limit catalytic conversion of larger molecules over the active sites located inside the zeolite crystallites and which can lead to significant coke deposition [7]. Several techniques have been used in order to improve the accessibility of zeolite active sites located within the zeolite crystals. One of the most common approaches to increase the accessibility of active sites for reacting molecules is the design of hierarchical zeolites. In addition to regular microporous networks, hierarchical zeolites contain a significant mesoporous volume. Extensive mesoporous network of hierarchical zeolite can significantly facilitate the diffusion of reacting molecules and products. There have been two main approaches for obtaining hierarchical zeolites [8]. The first one is called the "bottom-up" or templating strategy, which can be divided into (i) soft templating that includes amphiphilic organosilanes, quaternary ammonium-form surfactants and more recently ionic liquids [9,10], (ii) hard templating with typically carbon materials such as carbon blacks, carbon nanotube, carbon nanofibers, polymers or resin; and (iii) indirect templating. In the indirect templating method, the zeolite hierarchical structure is produced by partial "zeolitisation" of the amorphous walls of mesoporous materials.

The alternative "top-down" strategy addresses post-synthesis chemical modification of zeolite crystals by treatment with steam, acid or basic agents. These treatments lead to the extraction of aluminum and silicon atoms and modification of the zeolite framework [11].

Both "bottom-up" and "top-down" strategies for the synthesis of hierarchical zeolites have their advantages and drawbacks. Though the "bottom-up" methods generally yield more ordered mesoporous zeolites, high cost of templates and methodological difficulties restrict large-scale applications of templating methods, in particular at the larger industrial

93 scale. Creating mesoporosity in microporous materials using the "top-down" method
94 leads to less disordered mesoporous structures but at the same time, facilitates
95 manufacturing larger quantities of hierarchical zeolites. The major challenge in the design
96 of hierarchical zeolite using the "top-down" method is to keep high zeolite crystallinity
97 and micropore access during generation of the mesopores.

98 The top-down post-synthesis zeolite modifications can involve dealumination and
99 desilication [12]. Dealumination is a well-known post-synthesis method of removing
100 aluminum from zeolite structure with the use of chemical agents or by hydrothermal
101 treatment [13]. The goal of dealumination is to modify the Si/Al ratio in the zeolite
102 framework and zeolite acidity, while the zeolite mesoporous structure can be affected to
103 a variable degree depending on the treatment conditions. One of the major disadvantages
104 of dealumination is possible blockage of the zeolite micropores by the weakly acidic
105 extra-framework species. Though the presence of these extra-framework species and their
106 interaction with Brønsted acid sites can enhance the catalytic performance of zeolites in
107 some reactions [14,15], these species can also promote very significant carbon deposition,
108 which would lead to fast catalyst deactivation [16].

109 The "desilication" method, which preferentially extracts silicon atoms from the zeolite
110 framework, has been efficient for introducing additional mesopores, in particular, into
111 high silica zeolites such as ZSM-5, Beta and mordenite. During desilication, the Al atoms,
112 which were removed from the zeolite framework, can be subsequently reinserted into the
113 tetrahedral positions of mesopore walls forming acidic hydroxyls. The extraction of
114 silicon atoms from the framework is accompanied by partial breakdown of the zeolite
115 structure generating additional porosity, mainly in the mesoporous range. Depending on
116 the zeolite treatment conditions, dealumination or desilication may lead to significant
117 changes in the acidic properties of the zeolite, such as the number and strength of

118 Brønsted and Lewis acid sites [17]. Dealumination and desilication can produce different
119 effects on the zeolite smaller and larger crystals. A more significant amorphisation of the
120 zeolite is expected, when small size zeolite crystals are subjected to post-synthesis
121 treatments.

122 Dealumination and desilication could be used as complementary methods to control
123 zeolite acidity, to create porosity and to improve the transport properties. On one hand,
124 desilication leads to the abundant mesopore development, while on the other hand,
125 dealumination removes aluminum-rich species, which typically exhibit weaker Brønsted
126 acidity, and can result in extensive coke formation and pore blocking during catalytic
127 reactions. A combination of desilication and dealumination could therefore represent an
128 optimum strategy for the design of hierarchical zeolites with the best balanced
129 mesoporosity, crystallinity and acidity. Sun *et al.* [18] showed that combined
130 dealumination and desilication removed extra-framework aluminum, preserved intrinsic
131 microporosity, improved the acid site accessibility and catalytic performances in cracking
132 of heavy oils. This approach was also used by Feng [19] to obtain a hierarchical structure
133 with a partial breakdown of the crystallites and high amounts of both Brønsted and Lewis
134 acid sites. The synergetic effect of Brønsted and Lewis acid sites in a ZSM-5 catalyst
135 facilitated n-heptane conversion, while cleaner micropores and newly created
136 mesopores facilitated an increase in olefin selectivity and suppressed coke deposition.

137 Dealumination and desilication were used by Xin *et al.* [20] to fine-tune the amounts of
138 weak and strong acid sites in the zeolites. The acid strength had a major effect on the
139 product distribution for ethanol conversion to ethylene and diethyl ether over ZSM-5
140 catalysts, and the higher selectivity toward ethylene was associated with the increasing
141 weak acidity observed on these post-treated catalysts.

142 The present paper explores the effect of combining dealumination and desilication
143 treatments and their different sequences on the structure and acidity of the larger ZSM-5
144 zeolite crystals prepared from a sustainable source of silica such as coal fly ash. The
145 structural characterization data are discussed alongside the catalytic performance of the
146 zeolite material in anisole acylation with hexanoic acid. Acylation was used as a model
147 reaction probing the zeolite acidity on the external surface of the crystallites and in the
148 mesopores, which are developing during the zeolite post-synthesis treatments.

149

150 **2. Materials and methods**

151 *2.1 Material preparation*

152 The ZSM-5 zeolite was synthesized in our laboratories using fly ash as a silica source
153 derived from the combustion of Candiota mineral coal (RS, Brazil). The silica was
154 extracted by leaching the fly ash, which was generated during coal burning, using a
155 hydrothermal process in the presence of an alkaline solution of sodium hydroxide,
156 adapted from Cardoso *et al* [3]. **Figure 1** shows major steps involved in the extraction of
157 silica from fly ash. In a typical preparation, 25 g of fly ash was suspended in 150 mL of
158 an aqueous solution of NaOH in a 250-mL Schott bottles. Then, the flask containing the
159 NaOH and ash mixture was placed in an oven at a given temperature, so that the silica
160 leaching could occur.

161 After the leaching step, the suspension was subjected to vacuum filtration. Then, the pH
162 of the filtrate was adjusted to 7.0 using HCl in order to precipitate the silica. The
163 suspension was filtered again and the solid material, silica retained in the filter, was
164 washed with 200 mL of distilled water and dried in an oven at 100 °C for 12 h. In order
165 to evaluate the influence of the temperature, time and molar concentration of NaOH
166 solution on the coal ash silica extraction method and to define the best extraction

conditions, a rotational central composite design was used. Statistical analyses of the influence of the extraction parameters on the silica yield were performed with the software Statistica 8.0 (Stat Soft Inc., OK, USA), using the pure error that was calculated from the central point repetitions.

171

2.2. Zeolite synthesis

The zeolite synthesis was conducted in an autoclave at 190°C for 50 h in the presence of silica extracted from fly ash, aluminum sulfate, sodium sulfate, sodium hydroxide and N-butylamine ($\text{SiO}_2:0.02\text{Al}_2(\text{SO}_4)_3:0.3\text{C}_4\text{H}_{11}\text{N}:0.24\text{NaOH}:0.16\text{Na}_2\text{SO}_4:40\text{H}_2\text{O}$). After the hydrothermal synthesis, the zeolite sample was washed, dried and calcined to remove the organic template, and then converted into the H-form *via* ion exchange with ammonium nitrate followed by calcination at 450°C. The as-prepared ZSM-5 zeolite (with Si/Al ratio of 17 as determined by XRF) was then subjected to either dealumination or desilication, or both. The desilication treatment was performed in aqueous media: 1 g of the parent zeolite was added to 30 mL of solution of 0.2 M NaOH for 30 min at 65 °C, as reported by Groen [21]. After the alkaline treatment, the sample was washed, dried and calcined, then converted into H-form *via* ion exchange with ammonium nitrate followed by calcination at 450°C. The desilicated sample is referred to **DeSi**. Dealumination treatment of the parent zeolite was carried out in 90 mL of 0.1 M aqueous solution of oxalic acid for 3 h at 80 °C following the procedure described by Bonilla *et al* [22]. After the acid treatment, the sample was washed, dried and calcined at 450°C, and then converted into the H-form *via* ion exchange with ammonium nitrate followed by calcination at 450°C. This sample was labelled as **DeAl**. After the primary desilication or dealumination, a second treatment was performed: the desilicated zeolite was dealuminated and the dealuminated zeolite was subjected to desilication. The sample with the desilication as

192 the primary treatment was referred to **DeSiDeAl**, while the sample with the primary
193 dealumination treatment was labelled as **DeAlDeSi**.

194

195 *2.3 Catalyst characterization*

196 The sample chemical composition was determined by X-ray fluorescence (XRF) using a
197 M4 TORNADO (Bruker) spectrometer. The instrument was equipped with 2 anodes, a
198 rhodium X-ray tube (50 kV/600 mA, 30 W) and a tungsten X-Ray tube (50 kV/700 mA,
199 35 W), and a Silicon-Drift-Detector Si(Li) (<145 eV resolution at 100000 cps (Mn K)
200 with a Peltier cooling to 253°C). For sample characterization, the rhodium X-rays with a
201 poly-capillary lens enabling excitation of an area of 200 mm were used. The measurements
202 were conducted under vacuum (20 mbar). Quantitative analysis was performed using
203 fundamental parameters (standardless).

204 The BET apparent surface area, pore volume, and average pore diameter were determined
205 by low-temperature nitrogen adsorption using a Micromeritics ASAP 2000 automated
206 system. The apparent surface areas of the catalysts was calculated using the BET model
207 for the P/P_0 relative nitrogen pressure <0.04. The samples were degassed under vacuum
208 at <10 µmHg at 300°C for 4 h before N₂ physisorption. The total pore volume (TPV) was
209 calculated from the amount of vapor adsorbed at a relative pressure close to unity by
210 assuming that the pores are completely filled with the condensate in the liquid state. The
211 catalyst external surface area and micropore volume were calculated using the deBoer t-
212 plot method.

213 The samples were characterized by X-ray diffraction (XRD) using a D8 Advance
214 diffractometer equipped with an energy dispersive detector and a monochromatic CuK
215 radiation source. The samples were analyzed using a step of 0.02° with an acquisition
216 time of 0.5 s.

217 The electron micrographs were obtained by FEI-Quanta 200 scanning electron
 218 microscope (SEM) equipped with a field emission gun. Comparative characterization of
 219 the Brønsted and Lewis acid sites (BAS and LAS) in zeolites was carried out using
 220 transmittance FTIR measurements in the 6000-900 cm^{-1} spectral range utilizing pyridine
 221 (Py) and collidine (2, 4, 6-trimethyl pyridine) adsorption. Py was used for measuring the
 222 total number of BAS and LAS in the zeolites, while adsorption of collidine was used for
 223 evaluation of the number of acid sites on the zeolite external surface and mesopores as
 224 the relatively large size of collidine (7.9 Å) prevents its access to acid sites in the ZSM-5
 225 micropores. FTIR transmittance measurements were performed at $\sim 60^\circ\text{C}$ using catalyst
 226 self-supported disks activated at 450°C for 5 h in vacuum (with the temperature ramp of
 227 $1^\circ\text{C}/\text{min}$). FTIR spectra were collected using a Thermo iS10 spectrometer at a 4 cm^{-1}
 228 resolution (0.96 cm^{-1} data spacing). The spectra were analyzed using specialized Thermo
 229 software, Omnic. An excess of Py or collidine was admitted into the transmittance cell at
 230 150°C , in a stepwise manner until no changes were observed in the spectra. The saturated
 231 sample was then evacuated for 20 min at 150°C to remove physically adsorbed molecules.
 232 To quantify the number of acid sites from the area of the corresponding IR peaks of
 233 adsorbed Py, the following values of the molar absorption coefficients were used: (B,
 234 ZSM-5)=1.08 and (B, BEA)=1.16 $\text{cm} \mu\text{mol}^{-1}$ for Brønsted acid sites (peak at $\sim 1546 \text{ cm}^{-1}$
 235 ¹) and (L)=1.71 $\text{cm} \mu\text{mol}^{-1}$ for Lewis acid sites (peaks at $\sim 1455\text{-}1445 \text{ cm}^{-1}$). The (B,
 236 collidine)=10.1 $\text{cm} \mu\text{mol}^{-1}$ was used for calculating the concentration of BAS on the
 237 zeolite external surface from the spectra of adsorbed collidine [23,24]. Because of the
 238 steric hindrances introduced by methyl groups, the 2,4,6-trimethyl-pyridine did not
 239 interact with the Lewis acid sites.
 240 The ^{29}Si MAS NMR measurements were carried out utilizing a Bruker AVANCE
 241 spectrometer with the ^{29}Si Larmor frequency of 79.49 MHz and a 7 mm MAS rotor

242 spinning at 5 kHz and using a $\pi/2$ pulse length of 4.75 μ s. For the ^{27}Al resonance
243 measurement, the spectrometer used was Bruker AVANCE NEO operating at ^{27}Al
244 Larmor frequency of 208.48 MHz with a 3.2 mm MAS rotor spinning at 22 kHz and using
245 a $\pi/12$ pulse length to ensure a quantitative excitation of the central transitions [25]. The
246 analysis of the spectra was performed using DM Fit software [26]. The ^{27}Al and ^{29}Si
247 chemical shifts were referenced relative to 1 M $\text{Al}(\text{NO}_3)_3$ aqueous solution and $\text{Si}(\text{CH}_3)_4$,
248 respectively.

249

250 *2.4. Catalytic tests*

251 The activity of all catalysts was evaluated in the acylation reaction between anisole and
252 hexanoic acid according to the following protocol. The catalyst (20 mg) was added to a
253 mixture of anisole (2 g) and hexanoic acid (0.3 g) in a reflux reactor system (under
254 stirring) and heated at 180 $^{\circ}\text{C}$ for 2 h. The products were analyzed using gas-
255 chromatography.

256

257 **3. Results and Discussion**

258 *3.1. Optimization of silica extraction from fly ash*

259 First, the procedure for silica extraction from fly ash was optimized. The extraction
260 temperature, extraction time and molar concentration of NaOH solution were process
261 variables evaluated in this study (**Table S1, Supplementary Information (SI)**). The
262 analyzed response variable was the mass yield of extracted silica. The influence of the
263 NaOH concentration, the extraction time and temperature on the mass of the extracted
264 silica is displayed in **Figures S1, S2 and S3 (SI)**. The increase in time and the NaOH
265 concentration favor silica extraction, whereas the effect of the extraction temperature is
266 more complicated. The extraction yield reaches the maximum value at the temperatures

between 100 and 120 °C. Based on the data analysis using a regression model, the following optimum conditions were selected in order to boost the yield of silica: temperature of 100 °C, time of 72 h and NaOH concentration of 4 mol L⁻¹. Finally, the silica yield of 89.09 % was obtained. The XRD patterns of the extracted silica exhibiting a broad halo attributed to the amorphous phase are displayed in **Figure S4, SI**. The silica extracted from fly ash was amorphous. The elemental composition of the silica extracted from fly ash was evaluated using XRF (**Table S2, SI**). In addition to Si and O, the sample contained small amounts of aluminum (1.10 wt.%), sodium (2.97 wt. %) and potassium (0.48 wt.%).

3.2. Characterization of dealuminated and desilicated ZSM-5 zeolites

Figure 2 displays XRD patterns of the parent ZSM-5, dealuminated and desilicated zeolites. The intense XRD peaks characteristic of the MFI structure are observed in all samples. The sharp, well defined XRD peaks indicate the presence of relatively large zeolite crystallites. The dealumination and desilication treatments of the ZSM-5 catalyst do not result in any significant changes in the intensity, width and position of the XRD peaks, and no halo peaks, which can be attributed to the amorphous phase, have been detected. Overall, no noticeable decrease in the crystallinity or in the size of the crystalline domains of the zeolite catalyst has been observed after the post-synthesis treatments.

The SEM images of the parent zeolite, dealuminated and desilicated samples are shown in **Figure 3**. The parent zeolite contains cubic and prismatic crystals characteristic of the ZSM-5 structure with the relatively large average size of 5-7 μm (**Figure 3a**). Desilication results in appearance of clearly visible potholes and cracks on the surface of the single ZSM-5 crystals, while their overall morphology remains almost intact (**DeSi** sample, **Figure 3b**). Interestingly, the formation of potholes and cracks is less pronounced with

the dealuminated (**DeAl**) sample (**Figure 3c**). Zeolite treatment using combined dealumination and desilication leads to further noticeable changes: irregular shape of zeolite crystallites and the formation of leaf-type structure (**DeAlDeSi** and **DeSiDeAl** samples, **Figure 3d and e**).

Table 1 shows the chemical composition measured from XRF analysis and textural properties of the dealuminated and desilicated zeolites obtained from nitrogen adsorption-desorption isotherms. The Si/Al ratio is only slightly affected by dealumination and desilication. The nitrogen adsorption-desorption isotherms obtained for the studied zeolites are shown in **Figure 4**. The parent ZSM-5 sample displays a type I isotherm, which exhibits a sharp uptake at low relative pressure followed by a plateau with a hardly visible hysteresis at $P/P_0 > 0.5$. This type of isotherm is usually observed for microporous materials with negligible textural mesoporosity generated by aggregation of zeolite crystallites. The dealumination treatment does not significantly affect the shape of the nitrogen isotherm (**DeAl**, **Figure 4a**), indicating that the oxalic acid treatment does not create additional mesopores in the zeolite. In contrast to dealumination, zeolite desilication results in noticeable changes in the shape of adsorption isotherm (**DeSi**, **Figure 4b**), which presents a combination of type I and type IV isotherms showing a significant N_2 uptake at low relative pressure and a hysteresis loop at high relative pressure ($P/P_0 > 0.7$). This can be interpreted in terms of creating a new type of mesopores with relatively large pore sizes, which can correspond to the appearance of mesoporosity inside the zeolite crystallites or can arise from creating voids between and on the external surface of zeolites crystallites whose shape was modified by the treatment in alkaline media. The nitrogen adsorption data are consistent with the SEM images, which clearly show the formation of potholes and cracks following desilication in the **DeSi** sample (**Figure 3b**). Subsequent dealumination does not affect the shape of isotherms (**Figure**

318 **4b**), while desilication of the dealuminated sample (**Figure 4a**) yields an additional
319 hysteresis loop at $P/P_0 > 0.7$, which corresponds to the emergence of new mesopores or
320 voids between and on the external surface of the zeolite crystallites. Note that the BET
321 surface area is only slightly affected by the dealumination and desilication processes
322 (**Table 1**). The BJH mesopore distribution curves are shown in **Figure S5, SI**. They show
323 appearance of a peak corresponding to the pore radius from 30 to 60 Å corresponding to
324 the mesopores created by the zeolite post-treatments. Interestingly, the intensity of this
325 peak is lower and very small for the dealuminated DeAl zeolite. Desilication leads to a
326 noticeable increase in the intensity of this peak. The higher intensity is attained for
327 DeSideAl sample whose preparation involved primary desilication. These results indicate
328 that the desilication is the main process responsible for the introduction of mesoporosity
329 to the post-treated zeolite.

330 The ^{27}Al MAS-NMR and ^{29}Si MAS-NMR spectra of the studied ZSM-5 zeolites
331 displayed in **Figure 5** and the relative intensities of ^{27}Al MAS-NMR peaks summarized
332 in **Table 2** indicate the presence of mostly tetrahedrally coordinated framework Al atoms.
333 Indeed, the spectra show strong resonances with an isotropic chemical shift equal to 55.5
334 ppm, which is assigned to the four-fold coordinated Al atoms [27629]. There is also a
335 peak around 0 ppm representing approximately 10% of the aluminum atoms, which is
336 assigned to the six-fold coordinated extra-framework Al species. Its intensity is higher
337 for the zeolites subjected to combined dealumination and desilication. In addition to these
338 peaks, NMR spectrum of the parent ZSM-5 shows a peak at 28.0 ppm assigned to penta-
339 coordinated aluminum atoms [27]. The penta-coordinated Al species detected by ^{27}Al
340 MAS-NMR correspond to the Al atoms partially removed from the zeolite framework.
341 These species are present in the parent ZSM-5 zeolite. These labile species can easily
342 change their coordination during dealumination or desilication, for instance they can be

343 fully removed from or reinserted into the zeolite framework depending on the post-
344 synthesis modification conditions.

345 The ^{29}Si MAS NMR spectra of the studied zeolites (**Figure 5b**) exhibit resonances at -
346 106.2, -111.9 and -115.3 ppm which are characteristic of tetrahedral Si in ZSM-5 zeolites
347 that are surrounded by 3 Si and 1 Al or by 4 Si tetrahedra, ($\text{Q}_4(1\text{Al})$) or ($\text{Q}_4(0\text{Al})$) [30,31].
348 An example of the ^{29}Si MAS NMR spectrum deconvolution is given in **Figure S6, SI** and
349 the relative intensities of the individual peaks are summarized in **Table 3**. The most
350 prevalent type of SiO_4 tetrahedra is Q_4 . Dealumination and desilication only slightly
351 influence the relative intensity of ^{29}Si MAS NMR peaks. The Si/Al ratio calculated
352 according to Kilnowski *et al* [32] ($\text{Si}/\text{Al}=19\text{-}21$) is slightly higher than the value obtained
353 from the XRF analysis ($\text{Si}/\text{Al}=14\text{-}17$), confirming the presence of some extra-framework
354 aluminum species. Thus, the NMR results suggest a relatively small effect of
355 dealumination and desilication treatments on the bulk structure of the large ZSM-5 zeolite
356 crystals.

357 The acidity of the zeolites was evaluated using pyridine (Py) adsorption monitored by
358 FTIR spectroscopy. Following Py adsorption, the zeolite spectra (**Figure 6**) exhibit
359 characteristic bands at ~ 1545 and 1456 cm^{-1} attributed respectively to the pyridinium ion
360 (PyH^+) formed on BAS and to the Py molecules coordinated to LAS. Py adsorbed on both
361 LAS and BAS also displays a band at $\sim 1490\text{ cm}^{-1}$. **Table 4** shows the concentration of
362 BAS and LAS calculated from the intensity of the FTIR bands at ~ 1545 and 1456 cm^{-1} .
363 The amount of BAS (Py-BAS complexes) decreases in all zeolites after dealumination or
364 desilication. Interestingly, combined treatments of the zeolite using dealumination or
365 desilication (**DeAlDeSi** and **DeSiDeAl** samples) do not result in additional modification
366 of the zeolite acidity. At the same time, the concentration of LAS (Py-LAS complexes)
367 shows little change after the post-synthesis zeolite treatments.

368 Collidine adsorption over the zeolites gives rise to the band at $\sim 1634\text{ cm}^{-1}$ with a shoulder
 369 at $\sim 1649\text{ cm}^{-1}$ resulting from the interaction with BAS [33,34]; two low intensity bands
 370 at 1619 cm^{-1} and 1575 cm^{-1} are assigned to the probe adsorbed on Si-OH groups. The
 371 concentration of BAS measured from FTIR spectra of adsorbed collidine is shown in
 372 **Table 4**. Interestingly, zeolite desilication leads to a noticeable increase in the
 373 concentration of BAS on the external surface of the zeolites and in mesopores, while
 374 dealumination does not. This is also consistent with the appearance of defects on the
 375 surface of ZSM-5 crystallites after desilication observed by other techniques. Our data
 376 indicate it is the initial desilication treatment that is more important for improving access
 377 to the zeolite acid sites, probably, by creating additional mesopores near the external
 378 surface of the large ZSM-5 crystals, which is in agreement with BJH mesopore
 379 distribution data. In contrast, initial dealumination, even if it is producing additional
 380 mesopores near the external surface, seems to remove Al species and the associated acid
 381 sites. It should be noted, that the number of accessible external acid sites, generated as
 382 the result of any treatment, is rather small.

383 The surface composition of the zeolite crystals was also investigated using TOF-SIMS.
 384 The intensities of the identified Al- and Si-containing fragments are shown in **Table S3**,
 385 **SI**. The variation of the intensities of Al^+ and Si^+ fragments provides qualitative
 386 information about the chemical composition of the zeolite external surface. As expected,
 387 the zeolite dealumination results in a major decrease in the ratio of intensities of Al^+ to
 388 Si^+ fragments from 0.43 in **ZSM-5** to 0.11 in **DeAl**. This corresponds to the decrease in
 389 Al concentration on the zeolite external surface. Desilication results in a less significant
 390 decrease in the Al^+/Si^+ intensity ratio (from 0.43 in **ZSM-5** to 0.26 in **DeSi**). Subsequent
 391 dealumination of the desilicated **DeSi** sample leads to a further decrease in the Al
 392 concentration, while some increase in the Al^+/Si^+ intensity ratio was observed after

393 subsequent desilication of the **DeAl** sample. The Al^+/Si^+ intensity ratio drops from 0.23
394 to 0.13 in **DeSiDeAl**. Note that the variation of the Al^+/Si^+ intensity ratio on the zeolite
395 external surface observed by TOF-SIMS does not correlate with the Brønsted acidity of
396 the zeolite external surface measured from the FTIR spectra of adsorbed collidine. This
397 is indicative of the presence of significant amounts of extra-framework aluminum species
398 on the zeolite external surface, which do not exhibit noticeable Brønsted acidity.

399 Our results demonstrate that dealumination and desilication of the larger ZSM-5 zeolite
400 crystals principally modify the external surface of the zeolites, while the zeolite volume
401 is affected to a much lesser extent by these treatments. Indeed, the XRD data (**Figure 2**)
402 suggest that the post synthesis treatments of the large ZSM-5 zeolite crystals do not
403 significantly affect the zeolite bulk structure. The intensities of XRD peaks are almost
404 unaltered by dealumination, desilication or combined treatments. The concentration of
405 acid sites inside the zeolite crystallites measured by Py adsorption slightly decreases after
406 the dealumination, desilication or combined treatments (**Table 4**). Interestingly, the
407 amount of BAS and LAS is almost the same in the dealuminated and desilicated zeolites.

408 Both ^{27}Al and ^{29}Si MAS NMR show a minor effect of dealumination and desilication
409 conducted sequentially or separately on the coordination of aluminium or silicon atoms
410 in the zeolites. ^{27}Al MAS NMR (**Table 2**) shows little effects of different treatments on
411 the amount of octahedrally coordinated extra-framework aluminum species. ^{29}Si MAS
412 NMR (**Table 3**) shows only very slight effect of the post synthesis treatment on the local
413 environment of silicon species. The Si/Al ratios measured by both XRF and ^{29}Si MAS
414 NMR in the parent zeolite and in all dealuminated and desilicated samples are not affected
415 by the treatments. All these data suggest very small effect of dealumination, desilication
416 and combined treatments on the zeolite bulk structure.

417 It is important to note that the surface of the zeolite crystallites is affected to a much larger
418 extent. The SEM images (**Figure 3**) show a significant influence of desilication on the
419 shape of the zeolites crystallites. Unlike dealumination, the zeolite desilication results in
420 the formation of potholes, cracks and even leaf-type structures on the external surface of
421 the zeolites. The modification of the ZSM-5 zeolite crystallites is even more significant
422 in the samples subjected to a combination of desilication and dealumination. The SEM
423 results are consistent with nitrogen adsorption data. Interestingly, it is mostly desilication
424 that results in the appearance of additional large mesopores. These mesopores are
425 probably created by the voids between and on the external surface of the irregular zeolite
426 crystallites produced during the desilication. The acidity of the external surface of the
427 zeolites has been evaluated using the FTIR spectra of adsorbed collidine demonstrating
428 the emergence of BAS on the external surface on the desilicated zeolite sample, which
429 persist even after additional dealumination treatment. Our results strongly suggest that
430 dealumination using oxalic acid and desilication with sodium hydroxide start at the
431 external surface of the large ZSM-5 zeolite crystals. It should be noted that a prolonged
432 treatment under more severe dealumination or desilication conditions can lead to the
433 alternation of the bulk zeolite structure.

434 Acylation of anisole with hexanoic acid has provided additional information about the
435 acidity of the zeolite external surface and reactivity of the zeolite acid sites in the
436 dealuminated and desilicated zeolites (**Figure 7**). The large size of the reacting molecules
437 suggests that this reaction occurs on the external surface of the zeolite. The selectivity to
438 ortho-isomer was higher than 90% in all experiments and only traces of para- and meta-
439 isomers have been detected. No correlation has been found between the anisole
440 conversion and total amount of BAS in the zeolite as measured by Py adsorption (**Figure**
441 **8a**), confirming that the reaction does take place on the zeolite external surface. The

442 anisole conversion as a function of the Brønsted acidity on the external surface of the
443 large zeolite crystals (as measured by collidine adsorption) is shown in **Figure 8b**. Higher
444 anisole conversions are observed over the samples with a higher concentration of BAS
445 on the external surface of the ZSM-5 crystallites, which is more easily achieved by the
446 zeolite desilication. It is generally accepted that for high silica zeolites, such as ZSM-5
447 and beta with Si/Al ratio above ~10, the intrinsic strength of their Brønsted acid sites
448 does not change with a further increase in the Si/Al ratio, e.g. caused by dealumination.
449 There is also no indication that the Brønsted acid sites on the external surface of zeolite
450 crystals have a different strength as compared to those in the micropores of the same
451 zeolite.

452

453

454 **Conclusion**

455 A combination of characterization techniques has provided important new insights into
456 the phenomena occurring in the larger crystals of the ZSM-5 zeolite during dealumination
457 with oxalic acid and desilication with sodium hydroxide. Both desilication and
458 dealumination start at the external surface of the larger ZSM-5 zeolite crystals.
459 Desilication and, to a lesser extent, dealumination result in the appearance of potholes
460 and cracks on the external surface of larger ZSM-5 crystallites. These defects on the
461 zeolite external surface and voids between and on the external surface of the irregular
462 ZSM-5 crystals produced during the dealumination and desilication contribute to the
463 development of zeolite mesoporosity. XRD, ^{27}Al and ^{29}Si MAS NMR do not show any
464 noticeable modification of the zeolite bulk structure after the dealumination and
465 desilication treatments. Zeolite desilication leads to the appearance of additional Brønsted

466 acidity on the external surface of ZSM-5 zeolites, which contributes to a higher rate of
467 anisole acylation with hexanoic acid over these systems.

468

469 **Acknowledgement**

470 The authors are grateful to Laurence Burylo, Bertrand Revel and Joelle Thuriot for help
471 with XRD, NMR and XRF measurements. The authors thank International Cooperation
472 Program CAPES/COFECUB Foundation funded by CAPES ó Brazilian Federal Agency
473 for Support and Evaluation of Graduate Education within the Ministry of Education of
474 Brazil for providing a PhD stipend and financial support for this work. The Chevreul
475 Institute (FR 2638), Ministère de l'Enseignement Supérieur, de la Recherche et de
476 l'Innovation, Hauts-de-France Region and FEDER are acknowledged for supporting and
477 partially funding this work. The authors acknowledge financial support of the French
478 National Research Agency (DirectSynBioFuel project, Ref. ANR-15-CE06-0004 and
479 NANO4-FUT, Ref. ANR-16-CE06-0013).

480

481 **References**

- 482 [1] X. Querol, N. Moreno, J.C. Umana, A. Alastuey, E. Hernandez, A. Lopez-Soler,
483 F. Plana, Synthesis of zeolites from coal fly ash: an overview, *Int. J. Coal Geol.* 50
484 (2002) 4136423. doi:10.1017/CBO9781107415324.004.
- 485 [2] T. V. Ojumu, P.W. Du Plessis, L.F. Petrik, Synthesis of zeolite A from coal fly ash
486 using ultrasonic treatment ó A replacement for fusion step, *Ultrason. Sonochem.*
487 31 (2016) 3426349. doi:10.1016/j.ultsonch.2016.01.016.
- 488 [3] A.M. Cardoso, M.B. Horn, L.S. Ferret, C.M.N. Azevedo, M. Pires, Integrated
489 synthesis of zeolites 4A and Na-P1 using coal fly ash for application in the
490 formulation of detergents and swine wastewater treatment, *J. Hazard. Mater.* 287
491 (2015) 69677. doi:10.1016/j.jhazmat.2015.01.042.
- 492 [4] J.D.C. Izidoro, D.A. Fungaro, F.S. Dos Santos, S. Wang, Characteristics of
493 Brazilian coal fly ashes and their synthesized zeolites, *Fuel Process. Technol.* 97
494 (2012) 38644. doi:10.1016/j.fuproc.2012.01.009.
- 495 [5] L. Bieseki, F.G. Penha, S.B.C. Pergher, Zeolite A synthesis employing a brazilian
496 coal ash as the silicon and aluminum source and its applications in adsorption and
497 pigment formulation, *Mater. Res.* 16 (2012) 38643. doi:10.1590/S1516-
498 14392012005000144.
- 499 [6] B. Smit, T.L.M. Maesen, Towards a molecular understanding of shape selectivity,
500 *Nature.* 451 (2008) 6716678. doi:10.1038/nature06552.
- 501 [7] J.L. Atwood, J.W. Steed, eds., *Encyclopedia of Supramolecular Chemistry*, CRC
502 Press, 2004. doi:10.1081/E-ESMC.
- 503 [8] J. Li, M. Liu, X. Guo, S. Zeng, S. Xu, Y. Wei, Z. Liu, C. Song, Influence of Al
504 Coordinates on Hierarchical Structure and T Atoms Redistribution during Base
505 Leaching of ZSM-5, *Ind. Eng. Chem. Res.* (2018) acs.iecr.8b03539.

- doi:10.1021/acs.iecr.8b03539.
- [9] A. Sachse, C. Wuttke, E. Lissner, M. Oberson de Souza, Ordered Mesoporous ZSM-5 Employing an Imidazolium-Based Ionic Liquid, *Chem. - A Eur. J.* 20 (2014) 14996614999. doi:10.1002/chem.201404568.
- [10] A. Sachse, C. Wuttke, U. Díaz, M.O. de Souza, Mesoporous Y zeolite through ionic liquid based surfactant templating, *Microporous Mesoporous Mater.* 217 (2015) 81686. doi:10.1016/j.micromeso.2015.05.049.
- [11] A. Feliczak-Guzik, Hierarchical zeolites: Synthesis and catalytic properties, *Microporous Mesoporous Mater.* 259 (2018) 33645. doi:10.1016/j.micromeso.2017.09.030.
- [12] M.C. Silaghi, C. Chizallet, P. Raybaud, Challenges on molecular aspects of dealumination and desilication of zeolites, *Microporous Mesoporous Mater.* 191 (2014) 82696. doi:10.1016/j.micromeso.2014.02.040.
- [13] Y. Wei, T.E. Parmentier, K.P. de Jong, J. Ze evi , Tailoring and visualizing the pore architecture of hierarchical zeolites, *Chem. Soc. Rev.* 44 (2015) 723467261. doi:10.1039/C5CS00155B.
- [14] S. Schallmoser, T. Ikuno, M.F. Wagenhofer, R. Kolvenbach, G.L. Haller, M. Sanchez-Sanchez, J.A. Lercher, Impact of the local environment of Brønsted acid sites in ZSM-5 on the catalytic activity in n-pentane cracking, *J. Catal.* 316 (2014) 936102. doi:10.1016/j.jcat.2014.05.004.
- [15] S. Li, A. Zheng, Y. Su, H. Zhang, L. Chen, J. Yang, C. Ye, F. Deng, Brønsted/Lewis Acid Synergy in Dealuminated HY Zeolite: A Combined Solid-State NMR and Theoretical Calculation Study, *J. Am. Chem. Soc.* 129 (2007) 11161611171. doi:10.1021/ja072767y.
- [16] M. Hartmann, A.G. Machoke, W. Schwieger, Catalytic test reactions for the

- 531 evaluation of hierarchical zeolites, *Chem. Soc. Rev.* 45 (2016) 331363330.
532 doi:10.1039/C5CS00935A.
- 533 [17] C.S. Triantafillidis, A.G. Vlessidis, N.P. Evmiridis, Dealuminated H Y Zeolites:
534 Influence of the Degree and the Type of Dealumination Method on the Structural
535 and Acidic Characteristics of H Y Zeolites, *Ind. Eng. Chem. Res.* 39 (2000) 3076
536 319. doi:10.1021/ie990568k.
- 537 [18] H. Sun, P. Peng, Y. Wang, C. Li, F. Subhan, P. Bai, W. Xing, Z. Zhang, Z. Liu, Z.
538 Yan, Preparation, scale-up and application of meso-ZSM-5 zeolite by sequential
539 desilicationódealumination, *J. Porous Mater.* 24 (2017) 151361525.
540 doi:10.1007/s10934-017-0391-4.
- 541 [19] R. Feng, X. Yan, X. Hu, Y. Wang, Z. Li, K. Hou, J. Lin, Hierarchical ZSM-5
542 zeolite designed by combining desilication and dealumination with related study
543 of n-heptane cracking performance, *J. Porous Mater.* 25 (2018) 174361756.
544 doi:10.1007/s10934-018-0587-2.
- 545 [20] H. Xin, X. Li, Y. Fang, X. Yi, W. Hu, Y. Chu, F. Zhang, A. Zheng, H. Zhang, X.
546 Li, Catalytic dehydration of ethanol over post-treated ZSM-5 zeolites, *J. Catal.* 312
547 (2014) 2046215. doi:10.1016/j.jcat.2014.02.003.
- 548 [21] J.C. Groen, T. Bach, U. Ziese, A.M. Paulaime-Van Donk, K.P. De Jong, J.A.
549 Moulijn, J. Pérez-Ramírez, Creation of hollow zeolite architectures by controlled
550 desilication of A1-zoned ZSM-5 crystals, *J. Am. Chem. Soc.* 127 (2005) 107926
551 10793. doi:10.1021/ja052592x.
- 552 [22] A. Bonilla, D. Baudouin, J. Pérez-Ramírez, Desilication of ferrierite zeolite for
553 porosity generation and improved effectiveness in polyethylene pyrolysis, *J. Catal.*
554 265 (2009) 1706180. doi:10.1016/j.jcat.2009.04.022.
- 555 [23] N.S. Nesterenko, F. Thibault-Starzyk, V. Montouillout, V. V. Yushchenko, C.

556 Fernandez, J.-P. Gilson, F. Fajula, I.I. Ivanova, The use of the consecutive
 557 adsorption of pyridine bases and carbon monoxide in the IR spectroscopic study
 558 of the accessibility of acid sites in microporous/mesoporous materials, *Kinet.*
 559 *Catal.* 47 (2006) 40648. doi:10.1134/S0023158406010071.

560 [24] T. Onfroy, G. Clet, M. Houalla, Quantitative IR characterization of the acidity of
 561 various oxide catalysts, *Microporous Mesoporous Mater.* 82 (2005) 996104.
 562 doi:10.1016/j.micromeso.2005.02.020.

563 [25] A. Samoson, E. Lippmaa, Excitation phenomena and line intensities in high-
 564 resolution NMR powder spectra of half-integer quadrupolar nuclei, *Phys. Rev. B.*
 565 28 (1983) 656766570. doi:10.1103/PhysRevB.28.6567.

566 [26] D. Massiot, F. Fayon, M. Capron, I. King, S. Le Calvé, B. Alonso, J.-O. Durand,
 567 B. Bujoli, Z. Gan, G. Hoatson, Modelling one- and two-dimensional solid-state
 568 NMR spectra, *Magn. Reson. Chem.* 40 (2002) 70676. doi:10.1002/mrc.984.

569 [27] J. Klinowski, Applications of solid-state NMR for the study of molecular sieves,
 570 283 (1993).

571 [28] M. Haouas, F. Taulelle, C. Martineau, Recent advances in application of ^{27}Al
 572 NMR spectroscopy to materials science, *Prog. Nucl. Magn. Reson. Spectrosc.* 946
 573 95 (2016) 11636. doi:10.1016/j.pnmrs.2016.01.003.

574 [29] P. Sazama, E. Tabor, P. Klein, B. Wichterlova, S. Sklenak, L. Mokrzycki, V.
 575 Pashkkova, M. Ogura, J. Dedeczek, Al-rich beta zeolites . Distribution of Al atoms
 576 in the framework and related protonic and metal-ion species, *J. Catal.* 333 (2016)
 577 1026114. doi:10.1016/j.jcat.2015.10.010.

578 [30] J. Pérez Pariente, M. Sánchez-Sánchez, eds., *Structure and Reactivity of Metals in*
 579 *Zeolite Materials*, Springer International Publishing, Cham, 2018.
 580 doi:10.1007/978-3-319-98905-1.

- 581 [31] B. Rhimi, M. Mhamdi, V.N. Kalevaru, A. Martin, Synergy between vanadium and
582 molybdenum in bimetallic ZSM-5 supported catalysts for ethylene ammoxidation,
583 RSC Adv. 6 (2016) 65866665878. doi:10.1039/C6RA09736G.
- 584 [32] B. Sulikowski, J. Klinowski, Dealumination of zeolites with silicon tetrachloride
585 vapour. Part 6.-Zeolites Li, Na-X and Li, Na-Y, J. Chem. Soc. Faraday Trans. 86
586 (1990) 1996204. doi:10.1039/FT9908600199.
- 587 [33] F. Thibault-Starzyk, I. Stan, S. Abelló, A. Bonilla, K. Thomas, C. Fernandez, J.-P.
588 Gilson, J. Pérez-Ramírez, Quantification of enhanced acid site accessibility in
589 hierarchical zeolites ó The accessibility index, J. Catal. 264 (2009) 11614.
590 doi:10.1016/j.jcat.2009.03.006.
- 591 [34] C. Freitas, N.S. Barrow, V. Zholobenko, Accessibility and Location of Acid Sites
592 in Zeolites as Probed by Fourier Transform Infrared Spectroscopy and Magic
593 Angle Spinning Nuclear Magnetic Resonance, Johnson Matthey Technol. Rev. 62
594 (2018) 2796290. doi:10.1595/205651318X696792.
- 595
- 596

597

Table 1. Textural properties and chemical composition of the ZSM-5 zeolites.

	$S_{\text{BET}}^{\text{a}}$ ($\text{m}^2 \cdot \text{g}^{-1}$)	S_{ext} ($\text{m}^2 \cdot \text{g}^{-1}$)	$V_{\text{meso}}^{\text{a}}$ ($\text{cm}^3 \cdot \text{g}^{-1}$)	$V_{\text{micro}}^{\text{a}}$ ($\text{cm}^3 \cdot \text{g}^{-1}$)	Si/Al from XRF
ZSM5	460	109	0.067	0.133	17.0
DeSi	453	125	0.068	0.132	14.5
DeAl	443	124	0.060	0.129	14.2
DeSiDeAl	448	130	0.077	0.129	15.1
DeAlDeSi	480	143	0.080	0.137	14.6

598

599 **Table 2.** Fractions of aluminum atoms in different coordinations from ^{27}Al MAS NMR.

	Al^{IV}	Al^{V}	Al^{VI}
	56 ppm	28 ppm	0 ppm
ZSM-5	82	9	9
DeSi	92		8
DeAl	92		8
DeSiDeAl	91		9
DeAlDeSi	93		7

600

601

602

603

604

605

606

607

608 **Table 3.** Integrated intensity (%) of the ^{29}Si MAS-NMR peaks relating Si(nAl) building
 609 units and Si/Al ratio calcuted from ^{29}Si MAS-NMR.

	Si(1Al)	Si(0Al)	Si(0Al)	Si/Al ratio
	-106.2 ppm	-111.9 ppm	-115.3 ppm	
ZSM5	21	63	16	19
DeSi	20	63	17	20
DeAl	20	62	18	20
DeSiDeAl	20	63	17	20
DeAlDeSi	19	64	17	21

610

611 **Table 4.** Concentration of Bronsted and Lewis acid sites in the ZSM-5 zeolites.

612

	Number of acid sites, mol.g ⁻¹		
	Pyridine		Collidine
	Brønsted ^a	Lewis ^a	Brønsted ^b
ZSM5	483	50	1
DeSi	332	40	3
DeAl	335	39	1
DeSiDeAl	363	51	6
DeAlDeSi	310	40	1

613 ^a obtained by IR spectroscopy with pyridine adsorption at 150°C

614 ^b obtained by IR spectroscopy with collidine adsorption at 150°C

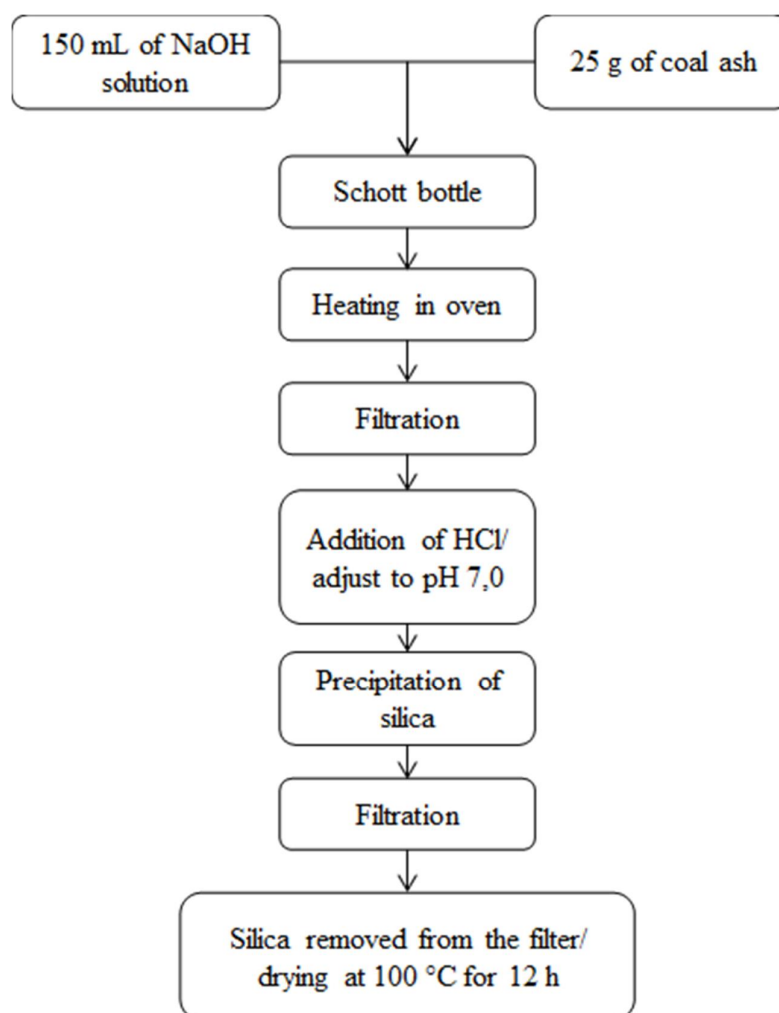
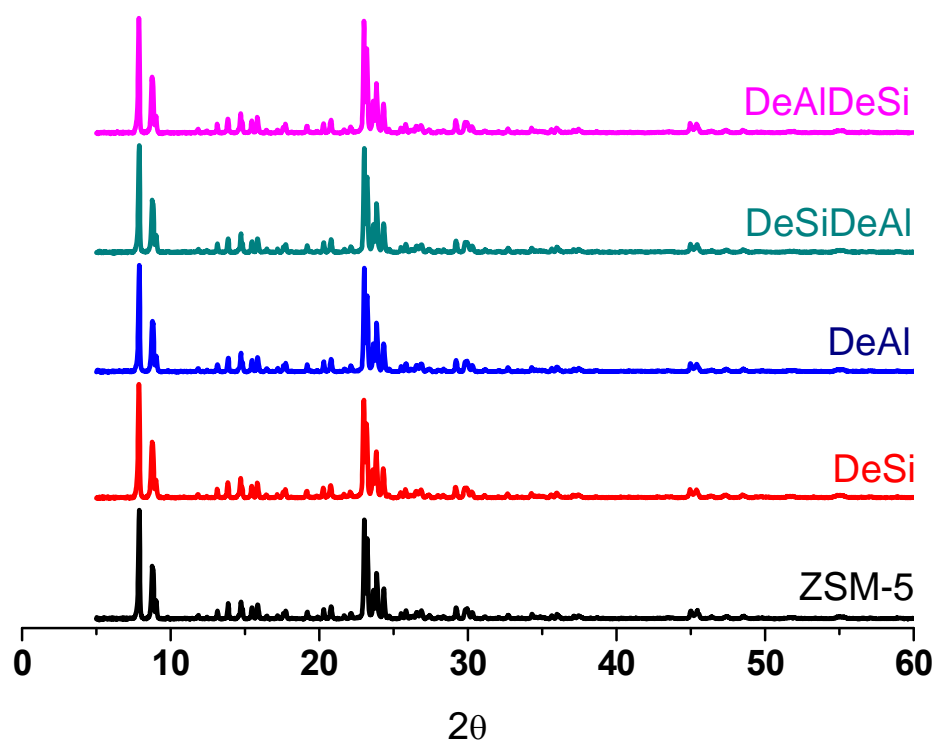


Figure 1. Schema of silica extraction from fly ash.

620

621

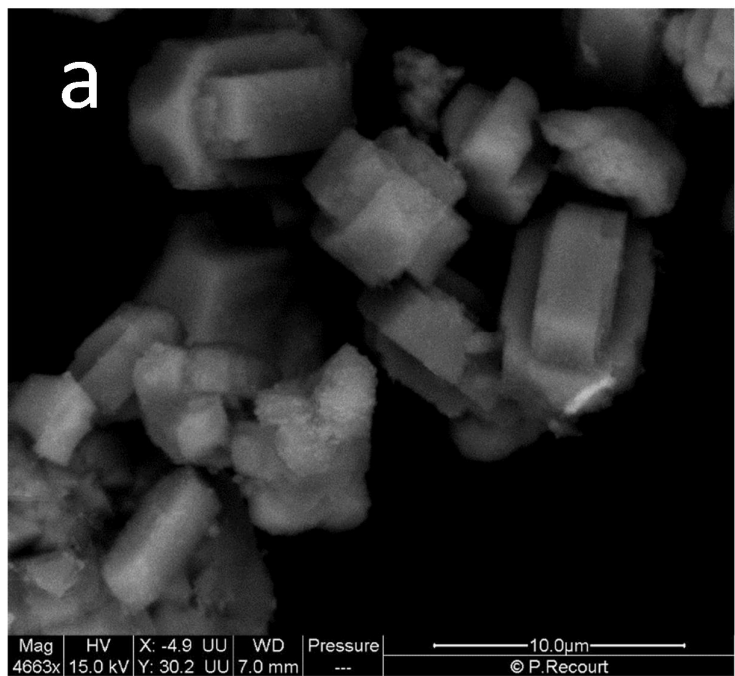


622

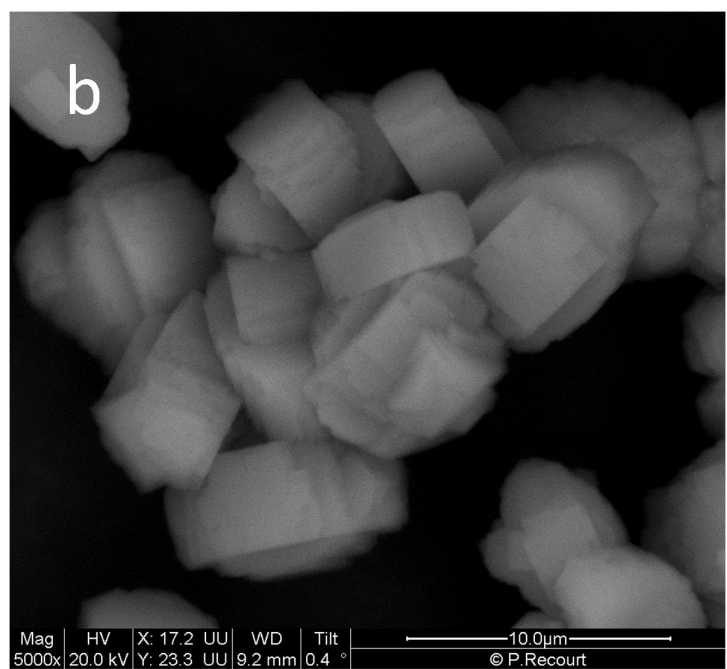
623

624 **Figure 2.** XRD patterns of the ZSM-5 zeolites

625

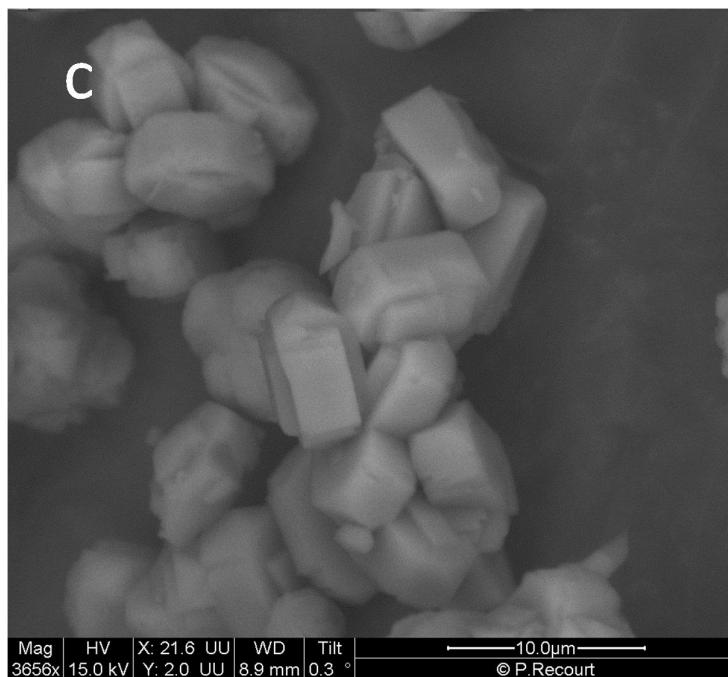


626



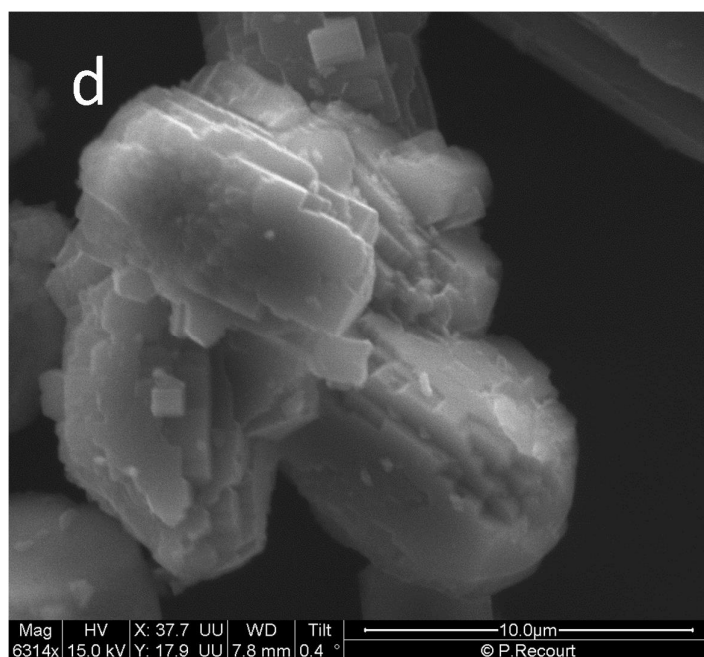
627

628



629

630



631

632



633

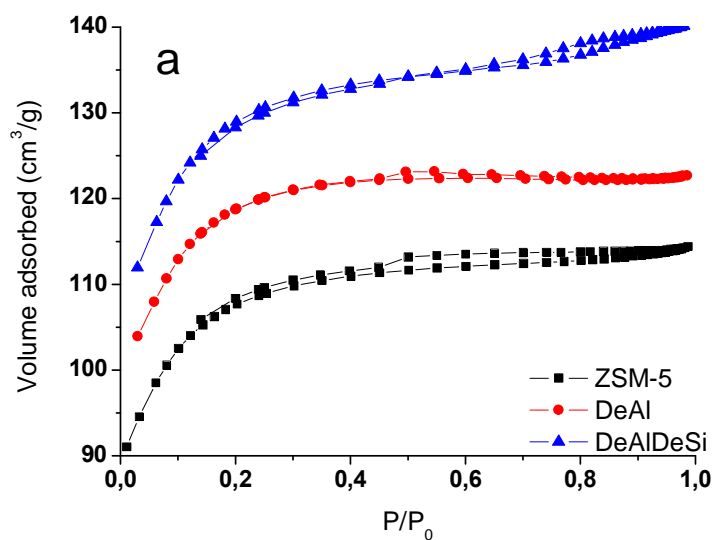
634

635 **Figure 3.** SEM images of the parent ZSM-5 zeolite (a), DeSi (b), DeAl (c), DeSiDeAl
636 (d), DeAlDeSi (e)

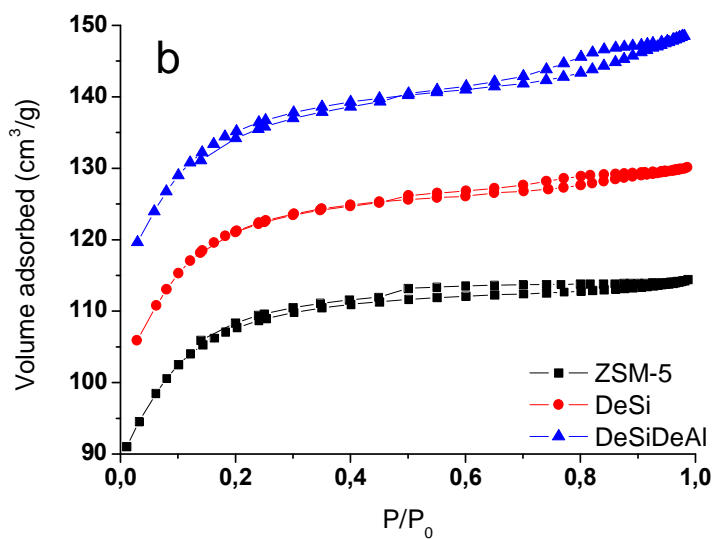
637

638

639



640

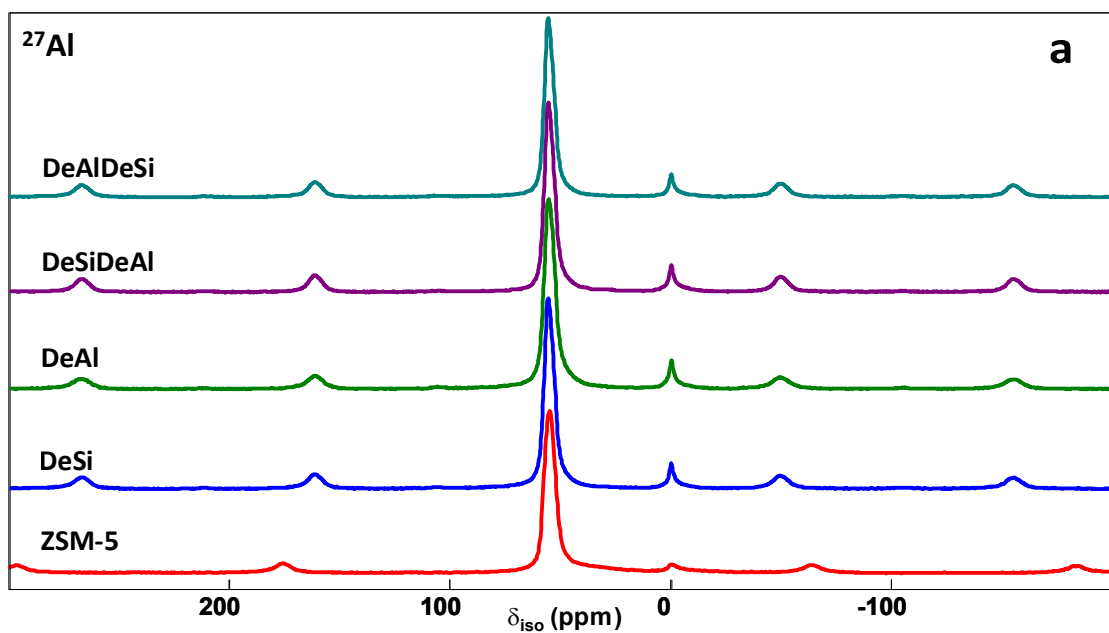


641

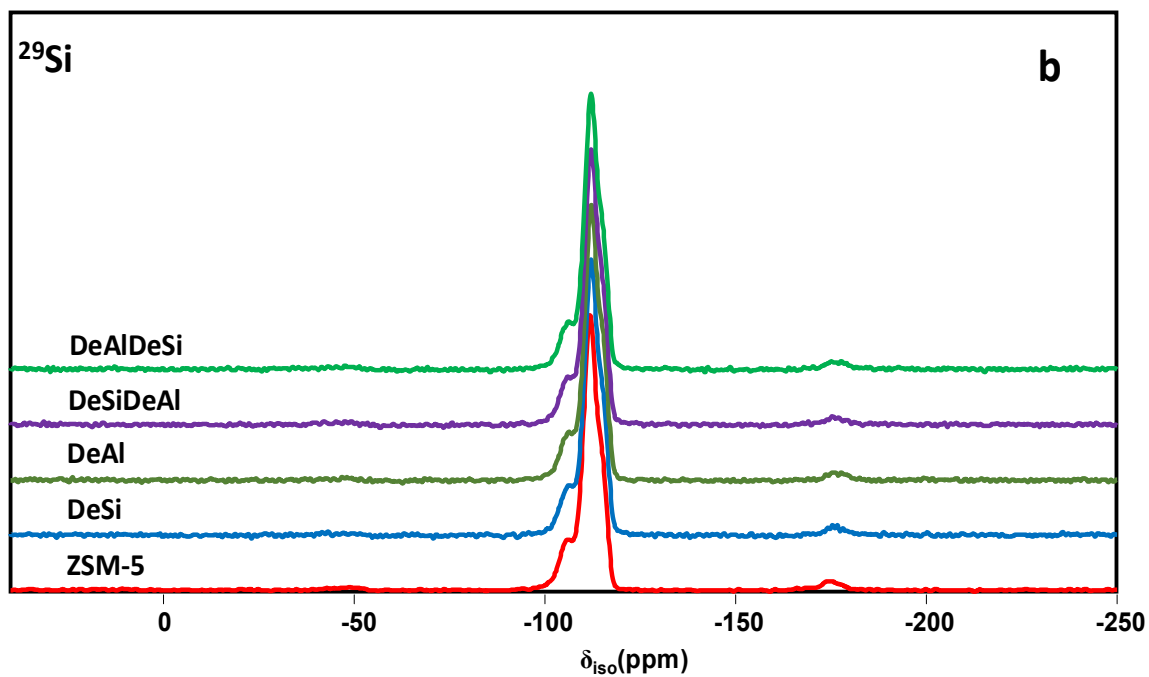
642 **Figure 4.** Isotherms of nitrogen adsorption-desorption over dealuminated and
 643 dealuminated-desilicated ZSM-5 (a), over desilicated and desilicated-dealuminated
 644 ZSM-5 (b).

645

646



647



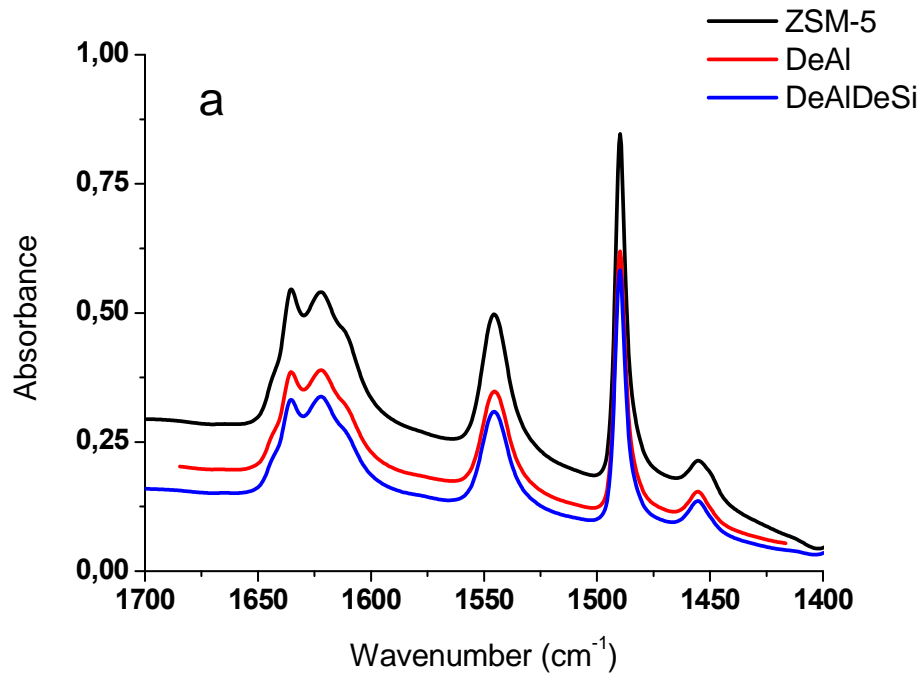
648

649

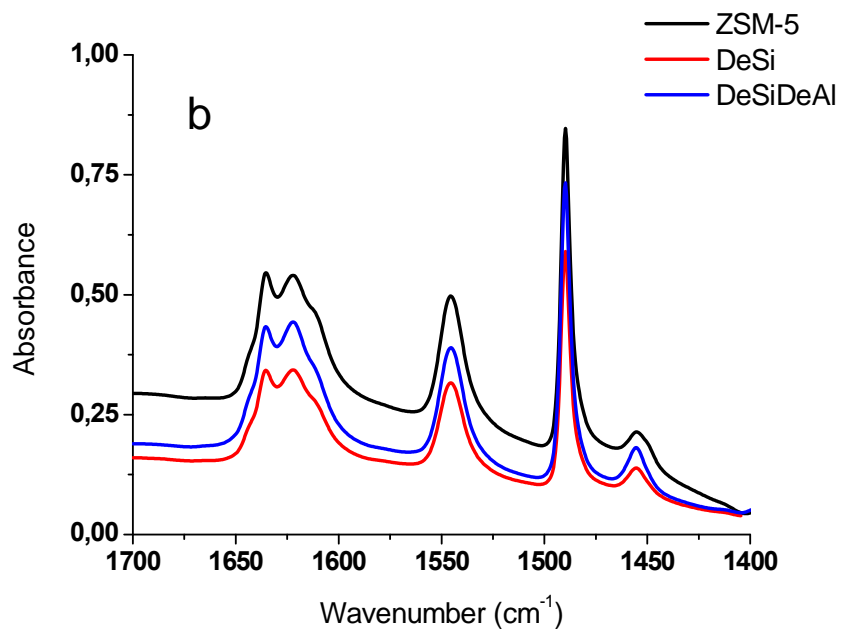
650 **Figure 5.** ^{27}Al MAS-NMR (a) and ^{29}Si MAS-NMR (b) spectra of ZSM-5 zeolites

651

652



653



654

655 **Figure 6.** FTIR spectra of Py adsorbed on over dealuminated and dealuminated-
 656 desilicated -ZSM-5 (a), over desilicated and desilicated-dealuminated ZSM-5 (b)

657

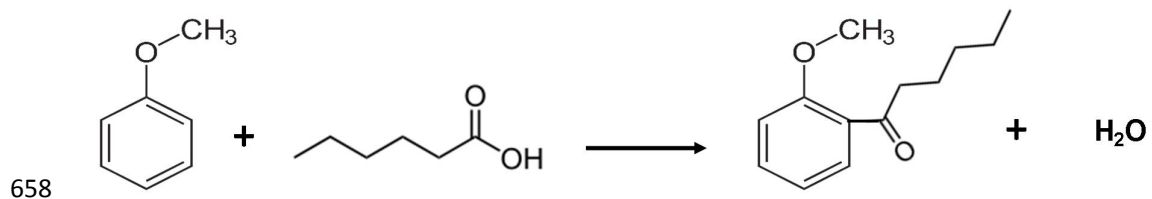


Figure 7. Acylation of anisole with hexanoic acid

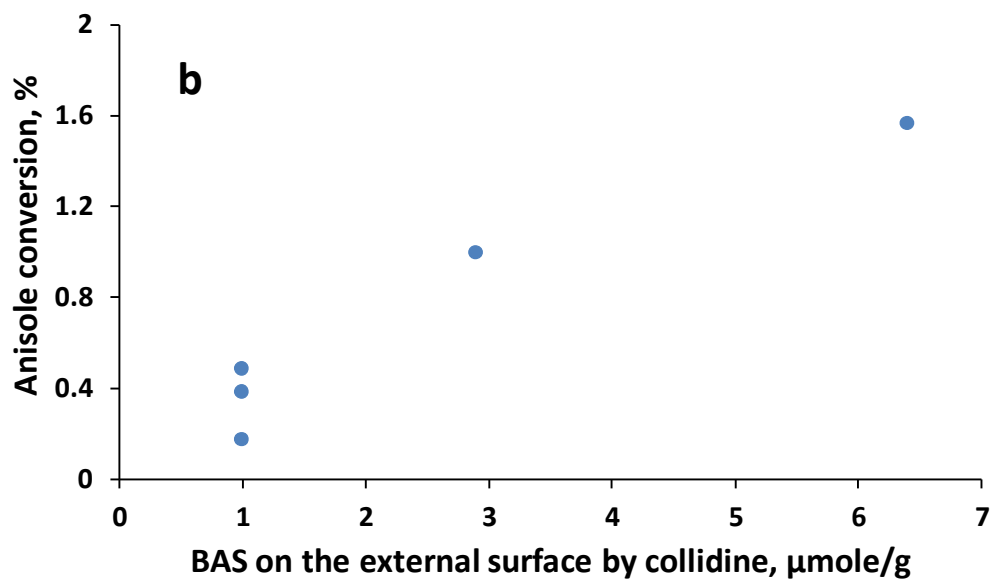
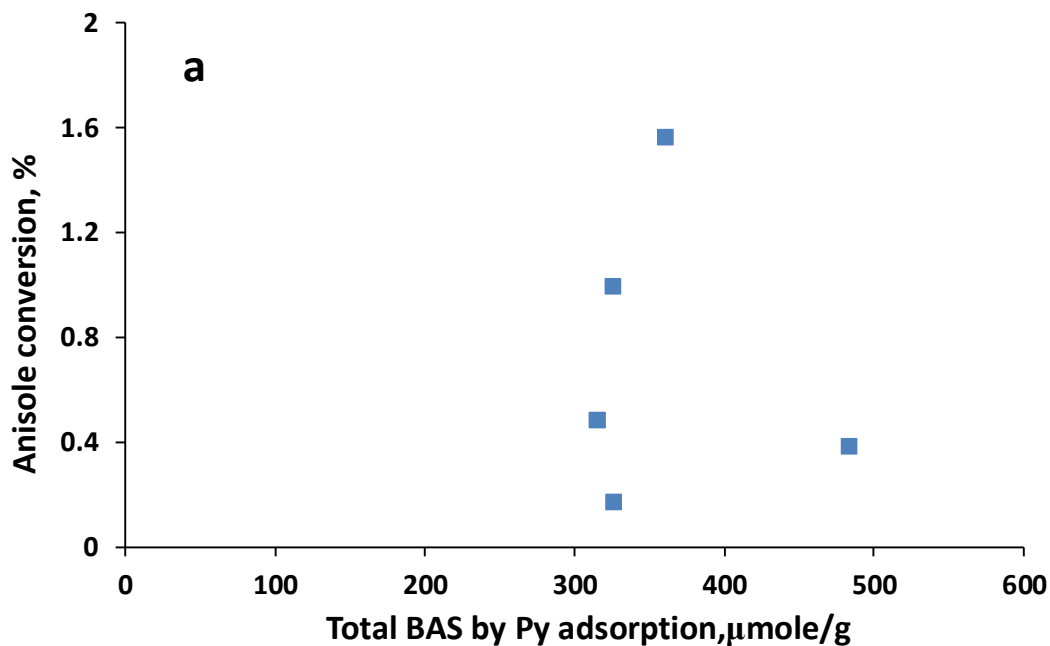


Figure 8. Anisole conversion over zeolites as a function of the total conversion of Bronsted acid sites measured by Py adsorption (a) and a concentration of Bronsted acid sites on the zeolite external surface (b).